

## Giant Colloidal Diffusivity on Corrugated Optical Vortices

Sang-Hyuk Lee and David G. Grier

*Department of Physics and Center for Soft Matter Research, New York University, New York, New York 10003, USA*

(Received 21 March 2006; published 16 May 2006)

A single colloidal sphere circulating around a periodically modulated optical vortex trap can enter a dynamical state in which it intermittently alternates between freely running around the ringlike optical vortex and becoming trapped in local potential energy minima. Velocity fluctuations in this randomly switching state still are characterized by a linear Einstein-like diffusion law, but with an effective diffusion coefficient that is enhanced by more than 2 orders of magnitude.

DOI: 10.1103/PhysRevLett.96.190601

PACS numbers: 05.40.-a, 05.60.-k, 82.70.Dd, 87.80.Cc

Brownian particles moving on tilted washboard potentials exhibit two well-characterized limiting behaviors [1]. When the potential energy wells are deeper than the thermal energy scale, diffusing particles become trapped in local minima. Their long-time self-diffusion coefficient vanishes in this limit. At the other extreme, tilting the washboard steeply enough to eliminate potential energy barriers allows particles to run freely downhill. Because diffusion is decoupled from translation at low Reynolds numbers, a freely running particle exhibits displacement fluctuations characterized by its equilibrium self-diffusion coefficient,  $D_0$ . Between the trapped and running limits, particles intermittently switch between the two states, drifting downhill at a mean speed set by the rate at which particles are thermally activated over barriers. The trajectory,  $x(t)$ , of such an intermittently trapped Brownian particle nevertheless is predicted [2–4] to satisfy the usual Einstein relation,

$$\lim_{t \rightarrow \infty} \langle x^2(t) \rangle - \langle x(t) \rangle^2 = 2Dt, \quad (1)$$

where  $D$  is an effective diffusion coefficient. Equally surprising is the prediction [2–4] that  $D$  can be enhanced by orders of magnitude over  $D_0$  at the crossover from locked to running states.

In this Letter, we provide experimental confirmation of substrate-mediated giant diffusivity by tracking the motions of a single colloidal sphere traveling on tilted washboard potentials created with corrugated optical vortex traps [5–7]. The optically driven particle undergoes normal diffusion even in the intermittent regime, with an effective diffusion coefficient that increases more than a hundred-fold at the point of maximum intermittency.

Our samples consist of colloidal polystyrene spheres  $2a = 1.48 \mu\text{m}$  in diameter (Bangs Laboratories, lot number 6064) dispersed in water and confined within a glass sample volume formed by bonding a No. 1 coverslip to a microscope slide. This assembly is mounted on the stage of a Zeiss S100TV Axiovert inverted optical microscope for observation. Images are captured by an NEC TI-324II video camera and recorded on a Panasonic DMR-E100H digital video recorder for processing and analysis. The polystyrene spheres sediment into a layer roughly

200 nm above the coverslip [8]. Individual particles are clearly resolved with a  $100\times$  NA 1.4 SPlan-Apo oil immersion objective lens that also is used to project holographic optical traps [7,9–12] into the sample. We tracked particles' motions with 10 nm spatial resolution at 1/30 s intervals using standard methods of digital video microscopy [13]. From measurements on freely diffusing spheres, we estimate [13,14] a wall-corrected self-diffusion coefficient of  $D_0 = 0.19 \pm 0.02 \mu\text{m}^2/\text{s}$ .

Tilted washboard potentials were created from superpositions of ringlike optical traps known as optical vortices [15–17]. Each optical vortex in this superposition is formed from a helical mode of light [18] whose fields,

$$\psi_\ell(\mathbf{r}) = u(r)e^{i\ell\theta}, \quad (2)$$

are characterized by a radially symmetric amplitude profile,  $u(r)$ , and a phase  $\varphi(\mathbf{r}) = \ell\theta$  proportional to the angle  $\theta$  about the optical axis. The wave fronts of such a beam take the form of an  $\ell$ -fold helix whose pitch determines the radius,  $R_\ell$ , of the projected ring of light [5,19]. A typical optical vortex with  $\ell = 40$  and  $R_\ell = 4.2 \pm 0.1 \mu\text{m}$  appears in Fig. 1(a). The focused ring of light acts like an optical gradient force trap, drawing nearby dielectric particles to its circumference. The helical pitch also endows each photon in the beam with  $\ell\hbar$  orbital angular momentum [18] that can be transferred to an illuminated object. The resulting torque causes a trapped object to circulate around the ring [20].

Superposing optical vortices with opposite helicities,  $\ell$  and  $-\ell$ , creates corrugated optical vortices such as the examples in Figs. 1(b) and 1(c) whose circumferential profiles are sinusoidally modulated [6] with  $2\ell$  intensity maxima [7]. An even superposition creates a so-called optical cogwheel [21] consisting of bright spots arranged in a circle of radius  $R_\ell$ . This superposition carries no net orbital angular momentum and thus exerts no torque. A more general superposition,

$$\psi(\mathbf{r}) = \frac{\psi_\ell(\mathbf{r}) + \sqrt{\alpha}\psi_{-\ell}(\mathbf{r})}{\sqrt{1+\alpha}}, \quad (3)$$

still exerts a torque, but also has a sinusoidal corrugation whose depth is set by  $0 \leq \alpha \leq 1$ . The two limits,  $\alpha = 0$

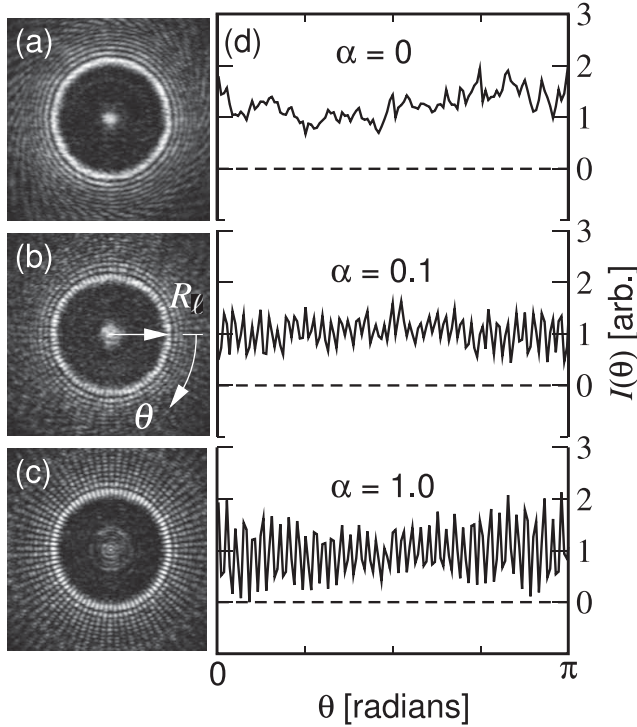


FIG. 1. (a) Optical vortex with  $\ell = 40$ . (b) and (c) Corrugated optical vortices,  $\alpha = 0.1$  and  $1.0$ , respectively. (d) Circumferential intensity profiles,  $I(\theta)$ , measured from (a), (b), and (c) at the radius of maximum intensity,  $R_\ell$ .

and  $\alpha = 1$ , correspond to an ideal optical vortex and an optical cogwheel, respectively. We vary  $\alpha$  by calculating phase-only holograms encoding the desired superposition using the direct search algorithm [12] and projecting the results with a Hamamatsu X7550 PAL-SLM spatial light modulator. Our experiments were performed with 1.5 W of laser light at a wavelength of  $\lambda = 532$  nm from a Coherent Verdi laser.

The images of corrugated optical vortices in Fig. 1 were obtained by placing a mirror in the microscope's focal plane and capturing the reflected light with the objective lens. Circumferential intensity profiles,  $I(\theta) = |\psi(R_\ell, \theta)|^2$ , measured from these images are plotted in Fig. 1(d) and reveal deviations in the depth of corrugation from the design to be smaller than 5%. Additional intensity variations of roughly 10% arise from imperfections in the optical train and so are independent of  $\alpha$ . These variations have an even smaller effect on the potential energy landscape experienced by the particle because the particle's finite extent tends to smooth them over [22,23].

A photon in the superposed beam has probability  $1/(1 + \alpha)$  of having orbital angular momentum  $+\ell\hbar$  and probability  $\alpha/(1 + \alpha)$  of having orbital angular momentum  $-\ell\hbar$ . The corrugated optical vortex therefore carries a local orbital angular momentum flux  $(\ell\lambda/c)[(1 - \alpha)/(1 + \alpha)]I(\theta)$ , where  $c$  is the speed of light. A fraction of this orbital angular momentum is transferred to a trapped object, and drives it around the ring. Circumferential intensity

gradients,  $\partial_\theta I(\theta)$ , modulate this torque, and also induce optical gradient forces. The overall circumferential force therefore has the form

$$F(\theta) = F_0[A(\alpha) + B(\alpha) \cos(2\ell\theta) + \eta(\theta)], \quad (4)$$

with  $A(\alpha) = (1 - \alpha)/(1 + \alpha)$  and  $B(\alpha) = 2\sqrt{\alpha(A^2 + \xi^2)}/(1 + \alpha)$ . The force scale,  $F_0$ , is proportional to the laser beam's power and depends on the particle's shape, size, and composition [22,23]. Given this, the washboard's tilt depends only on the excess,  $A(\alpha)$ , of right-helical photons in the corrugated optical vortex. The sinusoidal term, by contrast, includes a material- and geometry-dependent constant,  $\xi$ , accounting for the relative strength of the optical gradient force. We have omitted an irrelevant phase from the sinusoidal term's argument, and will ignore the landscape's roughness,  $\eta(\theta)$ , in what follows.

Figure 2 shows brief samples from typical single-particle trajectories in the trapped, running, and intermittent regimes. Here, we have plotted the angular displacement,  $\Delta\theta(t) = \theta(t + \delta t) - \theta(t)$  over the period  $\delta t = 1/30$  s of one video frame. The driving term vanishes in the cogwheel limit,  $\alpha = 1$ , and the particle remains trapped in a single local minimum of the potential, where it undergoes thermally driven fluctuations about its equilibrium position. In the freely running limit,  $\alpha = 0$ , it circulates around the ring nearly 3 times a second. Periodic features in the running state's displacements result from the particle passing repeatedly over the disordered landscape,  $\eta(\theta)$ . From these, we estimate  $\langle |\eta(\theta)|^2 \rangle \approx 0.01$ . At intermediate values of  $\alpha$ , the particle makes thermally activated transitions between trapped and running states so that its trajectory is characterized by intermittent bursts of motion resembling random telegraph switching noise.

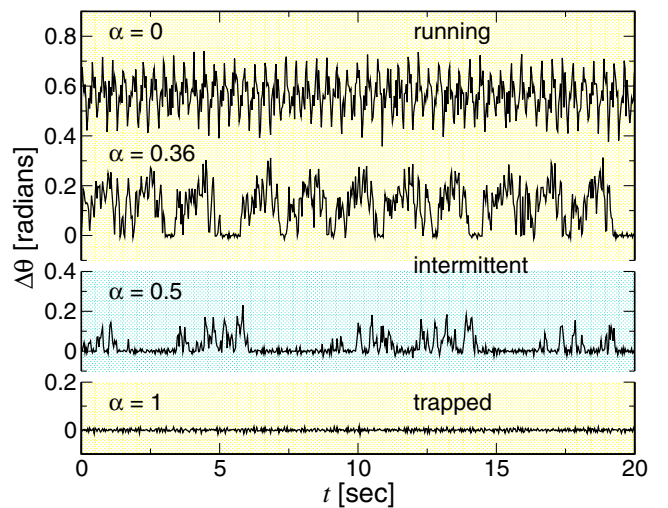


FIG. 2 (color online). Angular displacement over  $1/30$  s for a single  $1.48 \mu\text{m}$  diameter polystyrene particle circulating around corrugated optical vortices at  $\ell = 40$ ,  $P = 1.5$  W, and  $\alpha = 0, 0.36, 0.5$ , and  $1.0$ .

Averaging  $\Delta\theta(t)$  over a period long compared with the trajectory's correlation times yields an estimate for the mean circulation rate  $\omega(\alpha)$ , plotted in Fig. 3(a). The net orbital angular momentum flux driving this circulation decreases as  $\alpha$  increases, and we estimate the free circulation rate to be  $\omega_0(\alpha) = A(\alpha)\omega(0)$  from Eq. (4). This is drawn as a dashed curve in Fig. 3(a). The solid curve in Fig. 3(a) is a comparison to Stratonovich's exact expression for the mean drift velocity [3,4],

$$\omega(\alpha) = \frac{1 - e^{-2\pi\beta R_\ell F_0 A(\alpha)}}{R_\ell \int_0^{2\pi} I_+(\theta) \frac{d\theta}{2\pi}},$$

where  $I_\pm(\theta) = \frac{R_\ell}{D_0} e^{\pm\beta V(\theta)}$  (5)

$$\times \int_0^{2\pi} e^{\mp\beta V(\theta \mp \phi)} e^{-\beta R_\ell F_0 A(\alpha) \phi} d\phi$$

and where  $V'(\theta) = F_0[B(\alpha)\cos(2\ell\theta) + \eta(\theta)]$ .

Slow instrumental drifts in  $\omega(\alpha)$  amounting to a few percent over several minutes can be estimated [24] and subtracted off to reveal the linear growth of mean-squared positional fluctuations shown in the inset to Fig. 3(b). The associated effective diffusion coefficients,  $D(\alpha)$ , are plotted as triangles in Fig. 3(b). These values agree well with those obtained [3,4] from fluctuations in the time,  $T_j(\alpha)$ , required to complete the  $j$ th circuit,

$$D(\alpha) = 2\pi^2 R_\ell^2 \frac{\langle T_j(\alpha)^2 \rangle_j - \langle T_j(\alpha) \rangle_j^2}{\langle T_j(\alpha) \rangle_j^3},$$
 (6)

which are plotted as squares.

The measured effective diffusion coefficient agrees with the equilibrium value,  $D(\alpha) = D_0$ , when the particle is in the free-running state,  $\alpha < 0.2$ . Larger values of  $\alpha$  correspond to deeper corrugations that tend to trap the particle for longer periods. Longer periods of localization might be expected to reduce the particle's effective diffusion coefficient. Indeed,  $D(\alpha) = 0$  when the particle is trapped altogether for  $\alpha \geq 0.6$ . Instead, intermittent trapping dramatically increases the effective diffusion coefficient, with  $D$  exceeding  $100 D_0$  at  $\alpha = 0.4$ .

This extraordinary substrate-mediated enhancement of the effective diffusivity is accounted for by the exact formulation, analogous to Eq. (5), due to Reimann *et al.* [3,4],

$$D = D_0 \frac{\int_0^{2\pi} I_+^2(\theta) I_-(\theta) \frac{d\theta}{2\pi}}{\left[ \int_0^{2\pi} I_+(\theta) \frac{d\theta}{2\pi} \right]^3}. \quad (7)$$

Analysis of Eq. (7) reveals that peak diffusivity should occur when the driving force is just barely balanced by the periodic modulation. Neglecting  $\eta(\theta)$ , this occurs when  $\alpha$  satisfies  $A(\alpha) = B(\alpha)$ . Estimating the peak position to be  $\alpha = 0.41 \pm 0.01$ , we obtain  $\xi = 0.19 \pm 0.01$ . The sharp peak in  $D(\alpha)$  therefore can be used to probe how absorption and scattering transfer orbital angular momentum to objects trapped in optical vortices. The form for

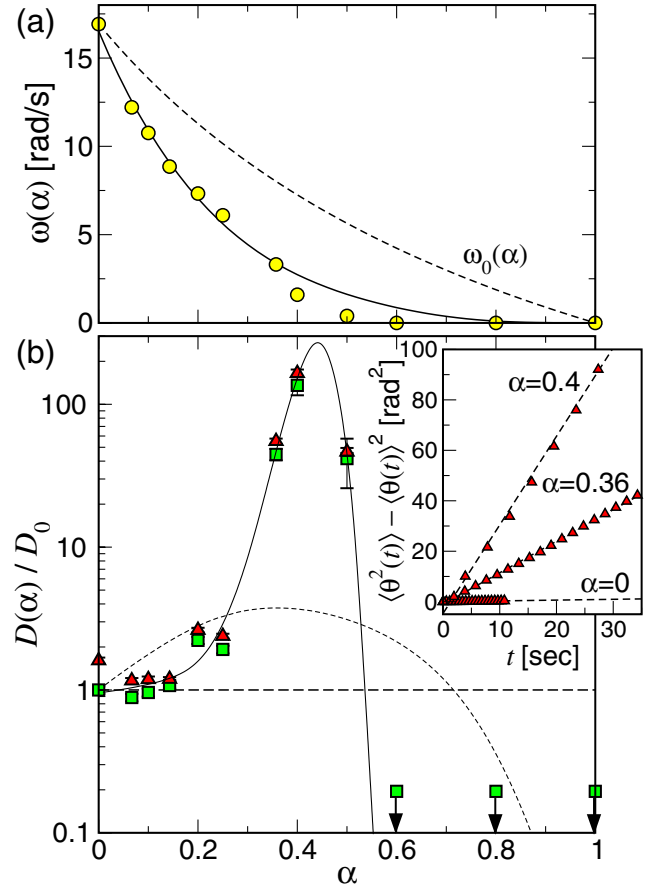


FIG. 3 (color online). (a) Dependence of circulation frequency on depth of corrugations. The solid curve is a fit to Eq. (5) yielding  $\xi = 0.19$  and  $F_0 = 1.5$  pN. The dashed curve is an estimate for  $\omega_0(\alpha)$  from Eq. (4). (b) Diffusion coefficients estimated from the inset plots of mean-squared displacements (triangles) show a dramatic enhancement around  $\alpha = 0.4$ . Squares denote equivalent results obtained from Eq. (6). Long-term self-diffusion coefficients are immeasurably small in the trapped state for  $\alpha \geq 0.6$ . The solid curve is a guide to the eye. The dashed curve is a comparison to Eq. (7) using parameters from (a).

$D(\alpha)$  predicted by Eq. (7) is plotted as the dashed curve in Fig. 3(b). Whereas Eq. (5) agrees well with  $\omega(\alpha)$ , Eq. (7) describes a much broader and weaker peak in  $D(\alpha)$  than is observed experimentally. It appears, therefore, that  $D(\alpha)$  is exceptionally sensitive to details of the potential energy landscape.

Histograms of angular displacements in Fig. 4 provide insights into this sensitivity. A freely running particle's displacements fall into a nearly Gaussian distribution, whose width and peak position both increase linearly in time. In the intermittent state, by contrast, particles spend much of their time localized in traps, so that the short-time displacement probability is highly non-Gaussian, as shown in Fig. 4(a). Because the potential energy landscape is periodic and the effective particle density is fixed, the displacement probability must evolve into a Gaussian distribution through the central limit theorem. This self-

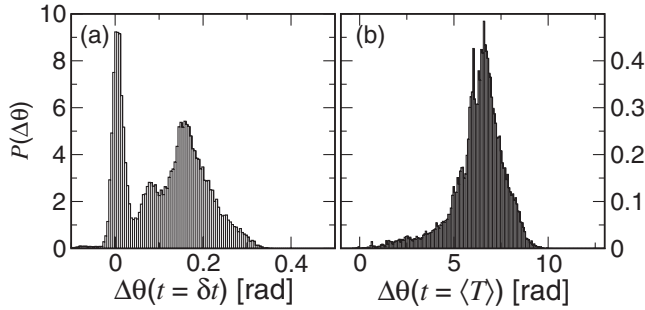


FIG. 4. Displacement histograms in the intermittent regime at  $\alpha = 0.36$ . (a) Short time,  $t = 33$  ms. (b) Long time,  $t = \langle T \rangle = 1.3$  s.

averaging can be effective over as little as a single mean first-passage time  $\langle T \rangle$ , as shown in Fig. 4(b). This accounts for the essentially normal diffusion evident in the inset to Fig. 3(b).

The peaked structure of the probability distribution in Fig. 4(a) also suggests a qualitative explanation for the overall enhancement of diffusivity. A particle undergoing intermittent transport has a probability  $p(t)$  of being trapped for time  $t$ , and a probability  $1 - p(t)$  of traveling with an angular speed  $\omega_0$  set by the washboard's overall tilt. The mean drift speed in this highly simplified two-state model is  $\omega = (1 - p)\omega_0$ . The running state is characterized by thermal fluctuations in the mean-squared angular speed of magnitude  $D_0/(R_\ell^2 t)$ . This, however, can be dominated by fluctuations due to thermally activated transitions between the stationary and running states. Taking  $t = \pi/(\ell\omega_0)$  to be the time required to travel between potential wells in the running state,

$$D \equiv \frac{R_\ell^2 t}{2} (\langle \omega^2 \rangle - \langle \omega \rangle^2) \quad (8)$$

$$= \frac{p(1-p)}{2} \frac{\pi R_\ell^2}{\ell} \omega_0 + (1-p)D_0. \quad (9)$$

The effective diffusion coefficient therefore can be made arbitrarily large by increasing  $\omega_0$ , with an upper limit set by the onset of inertial effects.

Giant diffusivity can degrade the performance of sorting methods such as gel electrophoresis and optical fractionation that exploit differential transport through a structured medium. In particular, the relative dispersal  $\Delta x/L$  of a sample that has traveled a mean distance  $L$  through the landscape at speed  $v$  is  $\sqrt{2D/(Lv)}$ , which can diverge with the effective diffusion coefficient  $D$ . This effect may be responsible for anomalous band broadening in electrochromatography [25]. Figure 3(b) demonstrates, however, that undesirable dispersal due to giant diffusivity can be overcome by more rapid driving, and that a small increase in driving force can have a disproportionately large effect on sorting resolution. On the other hand, substrate-mediated giant diffusivity should be useful for thoroughly mixing

and dispersing materials in microfluidic environments, and might also provide a strategy for enhanced mixing in granular materials.

We have benefited from conversations with Yael Roichman. This work was supported by the National Science Foundation through Grant No. DMR-0451589. S. L. acknowledges support of the Kessler Family Foundation.

- [1] H. Risken, *The Fokker-Planck Equation*, Springer Series in Synergetics (Springer-Verlag, Berlin, 1989), 2nd ed.
- [2] G. Constantini and F. Marchesoni, *Europhys. Lett.* **48**, 491 (1999).
- [3] P. Reimann, C. Van den Broeck, H. Linke, P. Hänggi, J. M. Rubi, and A. Pérez-Madrid, *Phys. Rev. Lett.* **87**, 010602 (2001).
- [4] P. Reimann, C. Van den Broeck, H. Linke, P. Hänggi, J. M. Rubi, and A. Pérez-Madrid, *Phys. Rev. E* **65**, 031104 (2002).
- [5] J. E. Curtis and D. G. Grier, *Phys. Rev. Lett.* **90**, 133901 (2003).
- [6] C.-S. Guo, X. Liu, J.-L. He, and H.-T. Wang, *Opt. Express* **12**, 4625 (2004).
- [7] S.-H. Lee and D. G. Grier, *Opt. Express* **13**, 7458 (2005).
- [8] S. H. Behrens and D. G. Grier, *J. Chem. Phys.* **115**, 6716 (2001).
- [9] E. R. Dufresne and D. G. Grier, *Rev. Sci. Instrum.* **69**, 1974 (1998).
- [10] J. E. Curtis, B. A. Koss, and D. G. Grier, *Opt. Commun.* **207**, 169 (2002).
- [11] D. G. Grier, *Nature (London)* **424**, 810 (2003).
- [12] M. Polin, K. Ladavac, S.-H. Lee, Y. Roichman, and D. G. Grier, *Opt. Express* **13**, 5831 (2005).
- [13] J. C. Crocker and D. G. Grier, *J. Colloid Interface Sci.* **179**, 298 (1996).
- [14] E. R. Dufresne, T. M. Squires, M. P. Brenner, and D. G. Grier, *Phys. Rev. Lett.* **85**, 3317 (2000).
- [15] H. He, N. R. Heckenberg, and H. Rubinsztein-Dunlop, *J. Mod. Opt.* **42**, 217 (1995).
- [16] N. B. Simpson, L. Allen, and M. J. Padgett, *J. Mod. Opt.* **43**, 2485 (1996).
- [17] K. T. Gahagan and G. A. Swartzlander, *Opt. Lett.* **21**, 827 (1996).
- [18] L. Allen, M. W. Beijersbergen, R. J. C. Spreeuw, and J. P. Woerdman, *Phys. Rev. A* **45**, 8185 (1992).
- [19] S. Sundbeck, I. Gruzberg, and D. G. Grier, *Opt. Lett.* **30**, 477 (2005).
- [20] H. He, M. E. J. Friese, N. R. Heckenberg, and H. Rubinsztein-Dunlop, *Phys. Rev. Lett.* **75**, 826 (1995).
- [21] A. Jesacher, S. Fuhpater, S. Bernet, and M. Ritsch-Marte, *Opt. Express* **12**, 4129 (2004).
- [22] K. Ladavac, K. Kasza, and D. G. Grier, *Phys. Rev. E* **70**, 010901(R) (2004).
- [23] M. Pelton, K. Ladavac, and D. G. Grier, *Phys. Rev. E* **70**, 031108 (2004).
- [24] C. Chatfield, *The Analysis of Time Series: An Introduction* (CRC Press, New York, 2003), 6th ed.
- [25] H. Rebscher and U. Pyell, *Chromatographia* **38**, 737 (1994).